Title

Structure of Guanylyl Cyclase Activator Protein 1 (GCAP1) Mutant V77E in a Ca2+-free/Mg2+-bound Activator State*

Journal

Journal of Biological Chemistry, 291(9)

ISSN

0021-9258

Authors

Lim, Sunghyuk

Peshenko, Igor V

Olshevskaya, Elena V

et al.

Publication Date

2016-02-01

DOI

10.1074/jbc.m115.696161

THE JOURNAL OF BIOLOGICAL CHEMISTRY VOL. 291, NO. 9, pp. 4429–4441, February 26, 2016

Structure of Guanylyl Cyclase Activator Protein 1 (GCAP1) Mutant V77E in a Ca^{2+}-free/Mg^{2+}-bound Activator State*

Received for publication, October 1, 2015, and in revised form, December 17, 2015 Published, JBC Papers in Press, December 24, 2015, DOI 10.1074/jbc.M115.696161

Sunghyuk Lim[‡], **Igor V. Peshenko**[§], **Elena V. Olshevskaya**[§], **Alexander M. Dizhoor**[§], **and James B. Ames**[‡1]

From the [‡]*Department of Chemistry, University of California, Davis, California 95616 and* [§]*Department of Research, Salus University, Elkins Park, Pennsylvania 19027*

GCAP1, a member of the neuronal calcium sensor subclass of the calmodulin superfamily, confers Ca^{2+}-sensitive activation of retinal guanylyl cyclase 1 (RetGC1). We present NMR resonance assignments, residual dipolar coupling data, functional analysis, and a structural model of GCAP1 mutant (GCAP1^{V77E}) in the Ca^{2+}-free/Mg^{2+}-bound state. NMR chemical shifts and residual dipolar coupling data reveal Ca^{2+}-dependent differences for residues 170–174. An NMR-derived model of GCAP1^{V77E} contains Mg^{2+} bound at EF2 and looks similar to Ca^{2+} saturated GCAP1 (root mean square deviations = 2.0 Å). Ca^{2+}-dependent structural differences occur in the fourth EF-hand (EF4) and adjacent helical region (residues 164–174 called the Ca^{2+} switch helix). Ca^{2+}-induced shortening of the Ca^{2+} switch helix changes solvent accessibility of Thr-171 and Leu-174 that affects the domain interface. Although the Ca^{2+} switch helix is not part of the RetGC1 binding site, insertion of an extra Gly residue between Ser-173 and Leu-174 as well as deletion of Arg-172, Ser-173, or Leu-174 all caused a decrease in Ca^{2+} binding affinity and abolished RetGC1 activation. We conclude that Ca^{2+}-dependent conformational changes in the Ca^{2+} switch helix are important for activating RetGC1 and provide further support for a Ca^{2+}-myristoyl tug mechanism.

Guanylyl cyclase activating proteins (GCAPs)[2] belong to the neuronal calcium sensor (NCS) branch of the calmodulin superfamily (1–3) and regulate Ca^{2+}-sensitive activity of retinal guanylyl cyclase (RetGC) in rod and cone cells (4–6). Phototransduction in retinal rods and cones is modulated by intracellular Ca^{2+} sensed by GCAPs (7, 8), and defects in Ca^{2+} signaling by GCAPs are linked to retinal diseases (9). GCAP proteins in the Ca^{2+}-free/Mg^{2+}-bound state activate RetGC (10), whereas Ca^{2+}-bound GCAPs inhibit RetGC at high Ca^{2+} levels maintained in the dark (11–13).

The GCAPs (GCAP1 (6), GCAP2 (14), GCAP3 (15), and GCAP4–8 (16) are all ~200-amino acid residue proteins containing a covalently attached N-terminal myristoyl group and four EF-hand motifs (EF1 through EF4; Fig. 1). Mg^{2+} binds to GCAP1 in place of Ca^{2+} when cytosolic Ca^{2+} levels are below 50 nM in light-activated photoreceptor cells (17). This Ca^{2+}-free/Mg^{2+}-bound GCAP1 is called the activator form because it activates RetGC (10, 18, 19). The x-ray crystal structure of Ca^{2+}-bound GCAP1 (20) and NMR structure of GCAP2 (21) showed that the four EF-hands form two semiglobular domains (EF1 and EF2 in the N-domain and EF3 and EF4 in the C-domain); Ca^{2+} is bound at EF2, EF3, and EF4, and the N-terminal myristoyl group in GCAP1 is buried inside the Ca^{2+}-bound protein flanked by hydrophobic residues at the N and C termini (see the *red residues* in Fig. 1). The structure of the physiological activator form of GCAPs (Mg^{2+}-bound/Ca^{2+}-free state) is currently unknown.

The structure of the Ca^{2+}-free/Mg^{2+}-bound activator state of GCAP1 has remained elusive, in part because it tends to aggregate under conditions for NMR or x-ray crystallography (22). Here, we present a NMR structural analysis of Ca^{2+}-free/Mg^{2+}-bound GCAP1 mutant that has Val-77 replaced by Glu (called GCAP1^{V77E}). The GCAP1^{V77E} mutant retains functional Mg^{2+} and Ca^{2+} binding with intact tertiary structure. However, unlike the dimeric wild type GCAP1, GCAP1^{V77E} is monomeric in solution and remains soluble under NMR conditions. Our NMR analysis indicates that Ca^{2+}-free/Mg^{2+}-bound GCAP1^{V77E} is overall structurally similar to that of Ca^{2+}-saturated GCAP1 (root mean square deviations of 2.0 Å), except that Mg^{2+} is bound at EF2, and the other EF-hands are unoccupied. The largest Ca^{2+}-dependent structural differences in GCAP1 are seen for residues in EF4 and the adjacent helical region (residues 164–174, called Ca^{2+} switch helix). We propose that the Ca^{2+} switch helix may serve as a conduit that relays Ca^{2+}-induced structural changes in EF4 to the RetGC binding site in the N-terminal domain, which provides further support of a Ca^{2+}-myristoyl tug mechanism (23).

Experimental Procedures

Expression and Purification of GCAP1 and Mutants—Mutations were introduced in a bovine GCAP1 coding plasmid using a "splice by overlap extension" approach as previously described (24). Myristoylated GCAP1 and its mutants were produced in *Escherichia coli* strain harboring yeast *N*-myristoyl

* This work was supported by National Institutes of Health Grants EY012347 (to J. B. A.), EY11522 (to A. M. D.), and RR11973 (UC Davis NMR). This work was also supported by a Pennsylvania Department of Health CURE Formula grant (to A. M. D.) The authors declare that they have no conflicts of interest with the contents of this article. The content is solely the responsibility of the authors and does not necessarily represent the official views of the National Institutes of Health.

The atomic coordinates and structure factors (code 2NA0) have been deposited in the Protein Data Bank (http://wwpdb.org/).

A complete list of NMR assignments for Ca^{2+}-free/Mg^{2+}-bound GCAP1^{V77E} has been deposited in the Biological Magnetic Resonance Bank (BMRB) (accession no. 26688).

[1] To whom correspondence should be addressed: Dept. of Chemistry, One Shields Ave., University of California, Davis, CA 95616. Tel.: 530-752-6358; Fax: 530-752-8995; E-mail: jbames@ucdavis.edu.

[2] The abbreviations used are: GCAP1, guanylyl cyclase activating protein 1; NCS, neuronal calcium sensor; HSQC, heteronuclear single quantum coherence; ITC, isothermal titration calorimetry; RDC, residual dipolar coupling; RetGC, retinal guanylyl cyclase; CaM, calmodulin.

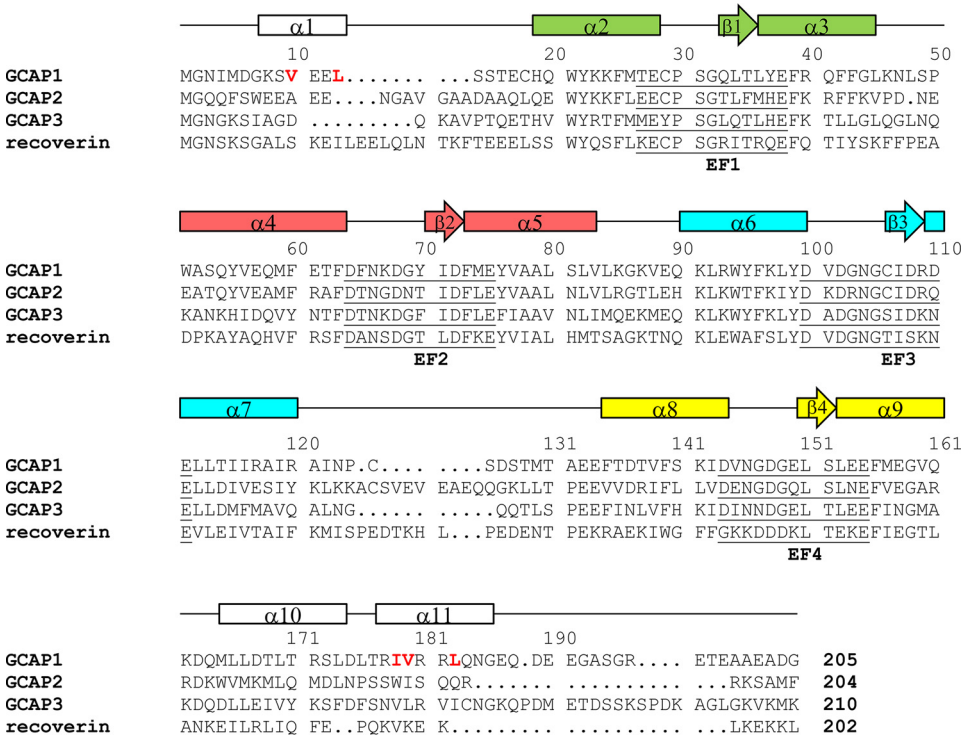

FIGURE 1. **Amino acid sequence alignment of bovine GCAP1, recoverin, and NCS-1.** Secondary structural elements (α-helices and β-strands) were derived from NMR analyses (22, 37). The four EF-hands (EF1, EF2, EF3 and EF4) are highlighted *green*, *red*, *cyan*, and *yellow*.

transferase and purified to homogeneity using a previously described method (10). The expression and purification of isotopically labeled GCAP1 and mutants were described previously (22, 25). Uniformly ^{15}N-labeled GCAP1, ^{15}N-labeled GCAP1^{V77E}, and triple-labeled ^{13}C,^{2}H,^{15}N-labeled GCAP1^{V77E} used in the NMR studies (0.5 mM) were dissolved in 5 mM Tris-d_{11} (pH 7.4), 5 mM $CaCl_2$, 5 mM $MgCl_2$, 5 mM dithiothreitol-d_{10}, and 93%/7% H_2O/D_2O.

Mutagenesis—Mutations were introduced in bovine GCAP1 cDNA by "splicing by overlap extension" technique using PCR reactions catalyzed by high-fidelity Phusion Flash polymerase (Finnzymes/Thermo Scientific). The resultant products were ligated into the NcoI/BamHI sites of *pET11d* (Novagen/Calbiochem) vector, sequenced, and transformed into expressing cell lines as described previously in detail (19).

Trp Fluorescence Spectroscopy—The intrinsic Trp fluorescence of GCAP1 and its mutants was recorded in the presence of variable-free Mg^{2+} and Ca^{2+} concentrations as previously described in detail (19, 23).

Ca^{2+} Binding Stoichiometry—The stoichiometry of Ca^{2+} binding to myristoylated and non-acylated GCAP1 and its mutants was determined using the fluorescent Ca^{2+} indicator dye method previously described in detail (19, 23) using Fluo-4FF (Molecular Probes/Fisher). Free Ca^{2+} in the reaction mixture was calculated using the formula $[Ca]_{free} = K_d \times (F - F_{min})/(100 - F)$, where F is the fluorescence intensity of the Ca^{2+} indicator in the assay mixture expressed as a percentage of the fluorescence of the Ca^{2+}-saturated indicator (recorded at the end of each experiment in 1 mM $[Ca]_{free}$), F_{min} is the fluorescence intensity of the Ca^{2+} indicator in the absence of Ca^{2+} and also expressed as a percentage of the fluorescence of the Ca^{2+}-saturated indicator, and K_d is a corrected constant of the indicator dye for Ca^{2+} (19). The fluorescence data were fitted by the equation $([Ca]_{bound}/[GCAP]) = N \times [Ca_{free}]^n/([Ca_{free}]^n + K_d^n)$, where $[Ca]_{bound}$ is the concentration of Ca^{2+} bound to GCAP1 calculated as $[Ca]_{bound} = [Ca]_{total} - [Ca]_{free}$, where N is the number of Ca^{2+} ions bound per molecule of GCAP at saturation, K_d is the apparent affinity of GCAP1 for Ca^{2+}, and n is the Hill coefficient. The data shown are representative from independent experiments producing virtually identical results.

Guanylyl Cyclase Assay—Recombinant human RetGC1 was expressed in HEK293 cells and assayed *in vitro* using [α-^{32}P]GTP as a substrate as previously described in detail (10, 23). Ca^{2+}/Mg^{2+}/ethylene glycol tetraacetic acid (EGTA) buffers for the assay were prepared and calibrated as previously described (10).

NMR Spectroscopy—Samples for NMR analyses were prepared by dissolving unlabeled, ^{15}N-labeled, ^{13}C,^{15}N-labeled, or ^{13}C,^{2}H,^{15}N-labeled GCAP1 proteins in 0.5 ml of 90% H_2O, 10% [^{2}H]H_2O containing 10 mM [$^2H_{11}$]Tris (pH 7.4) and either 5 mM $MgCl_2$ (Mg^{2+}-bound) or 5 mM $CaCl_2$ (Ca^{2+}-bound). All NMR experiments were performed at 37 °C on a Bruker Avance 800-MHz spectrometer equipped with a triple resonance cryoprobe and z axis gradient. NMR experiments and backbone assignments for Ca^{2+}-saturated GCAP1 were described elsewhere (22). Backbone NMR resonance assignments of the Ca^{2+}-free/Mg^{2+}-bound GCAP1^{V77E} activator state (Mg^{2+} bound at EF2) were obtained in this study by the analysis of three-dimensional NMR data as described previously (26). Two-dimensional ^{1}H,^{15}N HSQC with 2048 (^{1}H) × 256 (^{15}N) data points, three-dimensional HNCACB with 1024 (^{1}H) × 64 (^{15}N) × 120 (^{13}C)

TABLE 1
NMR structural statistics for Mg^{2+}-bound/Ca^{2+}-free $GCAP1^{V77E}$

NMR constraints	$GCAP1^{V77E}$
Distance restraints	
Inter-residue	
Sequential ($\|i-j\|=1$)	500
Medium range ($2 \le \|i-j\| \le 4$)	260
Long range ($\|i-j\| \ge 5$)	9
Mg^{2+}-EF-hand	5
Dihedral angle restraints	
ϕ	117
ψ	117
RDC restraints	41

data points, and three-dimensional HNCO with 2048 (^{1}H) × 64 (^{15}N) × 128 (^{13}C) data points were all performed on a triple-labeled $GCAP1^{V77E}$ sample using a 800-MHz Bruker NMR spectrometer equipped with a triple resonance cryogenic probe. In addition, three-dimensional HNCOCACB with 1024 (^{1}H) × 64 (^{15}N) × 128 (^{13}C) data points was performed on the triple-labeled sample using a 600-MHz Bruker NMR spectrometer equipped with a triple resonance cryogenic probe. ^{1}H,^{15}N residual dipolar coupling constants (D_{NH}) were measured with a ^{15}N-labeled $GCAP1^{V77E}$ (~0.3 mM) containing 12 mg/ml Pf1 phage (Asla Biotech) and using a two-dimensional IPAP (inphase/antiphase) ^{1}H,^{15}N HSQC experiment (27). Spectra were processed using NMRPipe software package (28) and analyzed using SPARKY.

NMR-guided Homology Modeling—An NMR-guided homology model structure of Mg^{2+}-bound/Ca^{2+}-free $GCAP1^{V77E}$ was generated based on NMR data (chemical shifts, residual dipolar couplings (RDCs) and NOEs) using the Xplor-NIH software suite (29, 30). A template structure for the model calculation was first built using SWISS-MODEL based on the x-ray crystal structure of Ca^{2+}-bound GCAP1 (PDB ID 2R2I). The N-terminal myristoyl group was attached to the template structure as it is in the crystal structure (PDB ID 2R2I). The three Ca^{2+} ions were deleted, and a single Mg^{2+} ion was added to the second EF-hand metal binding loop as described by Park *et al.* (31). The template structure of Mg^{2+}-bound $GCAP1^{V77E}$ then served as input for restrained molecular dynamics (32) followed by refinement (using refine.py) within the Xplor-NIH software suite (30). RDC and NMR restraints (NOEs and dihedral angles) were applied during the simulated annealing step. Dihedral angles were calculated by the Talos+ program (33). For under-assigned secondary structural motifs, theoretical restraints within the initial template structure were used to supplement the experimental restraints. Refinement of the final structure was initiated with high temperature annealing at 1000 K for 10 ps, and cooling from 1000 K to 25 K in 12.5 K steps. The duration of cooling dynamics run at each step was 0.2 ps. A total of 500 structures were obtained, and the 75 lowest energy structures were chosen to generate an energy-minimized average structure. The structural statistics are shown in Table 1.

Isothermal Titration Calorimetry—ITC experiments were performed using a VP-ITC calorimeter (Micro-Cal) at 30 °C, and data were acquired and processed with MicroCal software as described previously (34). Metal-free $GCAP1^{V77E}$ samples were prepared by exchanging protein into buffer containing 15 mM Tris-HCl (pH 7.5), 100 mM NaCl, and 1 mM β-mercaptoethanol. The metal-free $GCAP1^{V77E}$ in the sample cell (50 μM, 1.5 ml) was titrated with either Ca^{2+} (2 mM) or Mg^{2+} (40 mM) using 40 injections of 5 μl each.

Results

GCAP1 Mutant (V77E) Binds Functionally to Mg^{2+} and Ca^{2+}—ITC was used to monitor Mg^{2+} and Ca^{2+} binding to $GCAP1^{V77E}$ (Fig. 2). Titration of Mg^{2+} into apo$GCAP1^{V77E}$ produced an endothermic isotherm (Fig. 2*A*). Mg^{2+} binds to $GCAP1^{V77E}$ with an apparent dissociation constant (K_d) of 700 μM and enthalpy difference (ΔH) of +4.2 kcal/mol. The stoichiometry of Mg^{2+} binding was determined by analyzing ^{1}H,^{15}N HSQC NMR spectra of Mg^{2+}-bound $GCAP1^{V77E}$. NMR not only determined the number of Mg^{2+} ions bound per protein but also determined which particular EF-hands are bound to Mg^{2+} (35). The NMR spectrum of Ca^{2+}-free/Mg^{2+}-bound $GCAP1^{V77E}$ contains one downfield NMR peak at ~10.5 ppm assigned to Gly-69 (conserved glycine in EF2 binding loop), indicating that 1 Mg^{2+} is bound to $GCAP1^{V77E}$ at EF2. (Fig. 2*A*, *inset*). Thus, $GCAP1^{V77E}$ binds to Mg^{2+} with the same affinity and stoichiometry as wild type GCAP1 (25), which demonstrates that Ca^{2+}-free/Mg^{2+}-bound $GCAP1^{V77E}$ is structurally and functionally intact.

Titration of $CaCl_2$ into apo$GCAP1^{V77E}$ showed an ITC isotherm (Fig. 2*B*) with three separate phases that corresponded to Ca^{2+} binding at three EF-hand binding sites (EF2, EF3, and EF4). The Ca^{2+} binding isotherm of $GCAP1^{V77E}$ looked overall similar to that of wild type (25). The highest affinity site in $GCAP1^{V77E}$ (K_d = 0.08 μM and ΔH = −3 kcal/mol) exhibited binding energetics that are nearly identical to those of EF3 in wild type (25). Therefore, this highest affinity site in $GCAP1^{V77E}$ was assigned to EF3. The site with intermediate affinity (K_d = 0.2 μM and ΔH = +1.4 kcal/mol) was assigned to EF4 based on its similar binding affinity to EF4 in wild type under the conditions of microcalorimetry assay (25). By the process of elimination, the lowest affinity site in $GCAP1^{V77E}$ (K_d = 10 μM and ΔH = −0.5 kcal/mol) was assigned to EF2. The Ca^{2+} binding affinity for EF2 in $GCAP1^{V77E}$ is 10-fold weaker than that of wild type, consistent with the V77E mutation residing in EF2. The lower affinity Ca^{2+} binding to EF2 may also result from a loss of protein dimerization for $GCAP1^{V77E}$ compared with the dimeric wild type protein (22). For example, intermolecular dimer interactions involving EF2 could stabilize Ca^{2+} binding to EF2 in the dimeric wild type protein. Indeed, the ΔH for Ca^{2+} binding to both EF2 and EF4 in $GCAP1^{V77E}$ have opposite signs compared with that of wild type. The opposite sign of ΔH for both EF2 and EF4 in $GCAP1^{V77E}$ suggests that exposed residues in EF2 and EF4 might form Ca^{2+}-dependent intermolecular contacts with each other in the dimeric wild type protein that get disabled (or otherwise altered) in the monomeric $GCAP1^{V77E}$ (22).

The stoichiometry of Ca^{2+} binding was determined by analysis of ^{1}H,^{15}N HSQC NMR spectra of Ca^{2+}-bound $GCAP1^{V77E}$ (Fig. 2*B*, *inset*). Three downfield NMR peaks assigned to Gly-69 (EF2), Gly-105 (EF3), and Gly-149 (EF4) demonstrated that three Ca^{2+} ions are bound per protein at EF2, EF3, and EF4. Thus, $GCAP1^{V77E}$ binds to Ca^{2+} with the same stoichiometry and structure as wild type GCAP1 (17, 36).

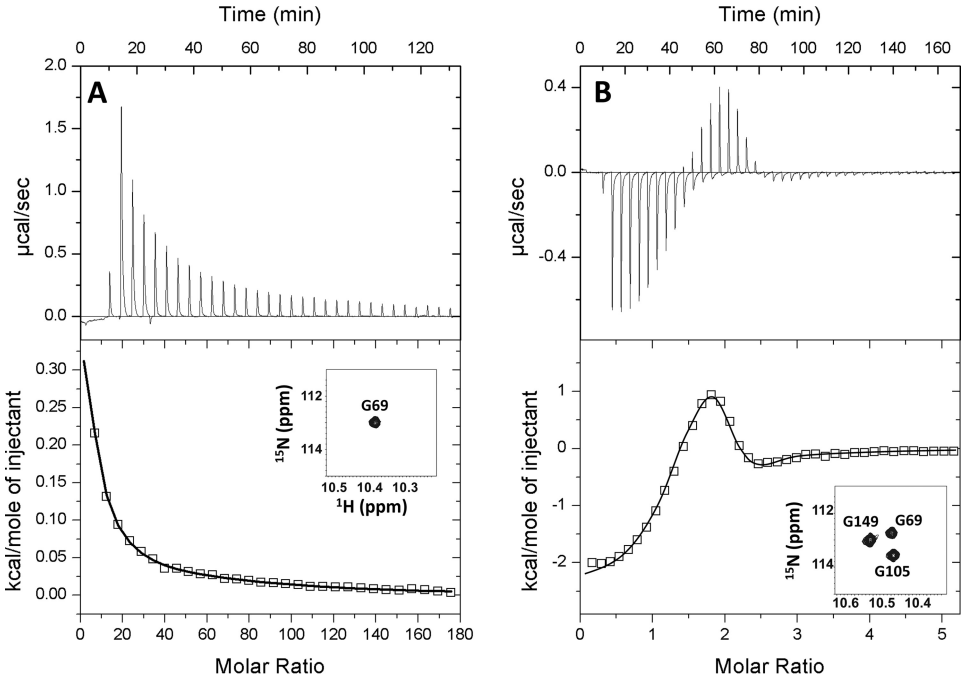

FIGURE 2. **GCAP1 mutant GCAP1^{V77E} binds to Mg^{2+} and Ca^{2+} as measured by ITC and NMR (*inset*).** ITC binding isotherms recorded at 30 °C are shown for Mg^{2+} binding (*A*) and Ca^{2+} binding (*B*) to GCAP1^{V77E}. Binding isotherms were fit to a sequential model (*solid line*), and fitting parameters are given in "Results." Downfield spectral regions of ^{1}H,^{15}N HSQC spectra of Mg^{2+}-bound GCAP1^{V77E} (*inset*, *A*) and Ca^{2+}-bound GCAP1^{V77E} (*inset*, *B*) are also shown. The downfield peak assigned to Gly-69 indicates Mg^{2+} is bound at EF2 (*inset*, *A*), whereas peaks assigned to Gly-69, Gly-105, and Gly-149 indicate Ca^{2+} is bound at EF2, EF3, and EF4.

NMR Assignments for Ca^{2+}-free/Mg^{2+}-bound GCAP1^{V77E}—NMR spectroscopy was used to demonstrate that GCAP1^{V77E} adopts a native tertiary structure as determined by comparing ^{1}H,^{15}N HSQC spectra of wild type protein (Fig. 3*A* and Ref 37) to that of GCAP1^{V77E} (Fig. 3, *B* and *C*). The peaks in the ^{1}H,^{15}N HSQC NMR spectra represent main chain and side-chain amide groups that provide a residue-specific fingerprint of the overall protein conformation. The resonance assignments for Ca^{2+}-saturated GCAP1^{WT} (37) match quite well with the spectrum of Ca^{2+}-saturated GCAP1^{V77E} (Fig. 3*C*), indicating that GCAP1^{V77E} is structurally intact. The NMR assignments for Ca^{2+}-free/Mg^{2+}-bound GCAP1^{V77E} are shown by the labeled peaks in Fig. 3*B*. The Ca^{2+}-free/Mg^{2+}-bound GCAP1^{V77E} forms a monomer in solution under NMR conditions (22), in contrast to Ca^{2+}-free/Mg^{2+}-bound wild type GCAP1 that tends to aggregate and/or form dimers under NMR conditions (22). The relative peak positions and spectral patterns overall look similar when comparing spectra of wild type (Fig. 3*A*) to that of GCAP1^{V77E} (Fig. 3*B*), indicating that Mg^{2+}-bound/Ca^{2+}-free GCAP1^{V77E} retains the same main chain fold compared with wild type. The monomeric state of GCAP1^{V77E} caused much sharper NMR line width s compared with that of dimeric wild type (Fig. 3, *A versus B*). The sharper NMR peaks observed for Ca^{2+}-free/Mg^{2+}-bound GCAP1^{V77E} allowed ~60% assignment of backbone resonances compared with <25% assignment for Ca^{2+}-free wild type and ~80% assignment for Ca^{2+}-saturated GCAP1 (37). The unassigned residues for GCAP1^{V77E} included the first 20 residues from the N terminus and unstructured regions (Lys-46–Trp-51, Met-74–Asp-108, Ile-119–Met-129, Asp-143–Leu-150, Arg-177–Gln-183). These unassigned residues have weak NMR intensities due to exchange broadening, suggesting that these residues undergo dynamical motions on the chemical shift time scale. The exchange broadening of residues at the domain interface in Ca^{2+}-free/Mg^{2+}-bound GCAP1 (residues Lys-91–Tyr-99) is similar to that seen in Ca^{2+}-free recoverin (38, 39).

Downfield-shifted NMR peaks at ~10.5 ppm for GCAP1^{V77E} are assigned to conserved glycine residues in the EF-hand Ca^{2+} binding loops and are characteristic of Ca^{2+}/Mg^{2+}-bound EF-hands. In Ca^{2+}-saturated GCAP1^{V77E} (Fig. 3*C*), three downfield peaks assigned to Gly-69 (EF2), Gly-105 (EF3), and Gly-149 (EF4) confirm that Ca^{2+} is bound at EF2, EF3, and EF4 as seen in the crystal structure (20). In Ca^{2+}-free/Mg^{2+}-bound GCAP1^{V77E} (Fig. 3*B*), one downfield peak assigned to Gly-69 (EF3) confirmed that Mg^{2+} is bound at EF2 as seen by fluorescence spectroscopy (10, 19).

NMR-derived Structural Model of Ca^{2+}-free/Mg^{2+}-bound GCAP1^{V77E}—The sequence-specific NMR assignments above for Ca^{2+}-free/Mg^{2+}-bound GCAP1^{V77E} and the secondary structure based on these assignments is summarized in Fig. 1. An NMR-derived structural model of Ca^{2+}-free/Mg^{2+}-bound GCAP1^{V77E} was calculated using NOE-based distances, NMR-derived dihedral angle restraints, and RDC data (Fig. 4) that served as input for restrained molecular dynamics structure calculations (see "Experimental Procedures"). Initial residual dipolar coupling magnitude and rhombicity were calculated by fitting the measured residual dipolar couplings to the calculated structure using the PALES program (40). The RDC-refined structures have a quality Q-factor of 0.28 and an R-factor of 0.995 (Fig. 4*C*). The overall secondary structure and topology of Mg^{2+}-bound GCAP1^{V77E} is similar to that found in the crystal structure of Ca^{2+}-bound GCAP1 (20). The NMR-derived

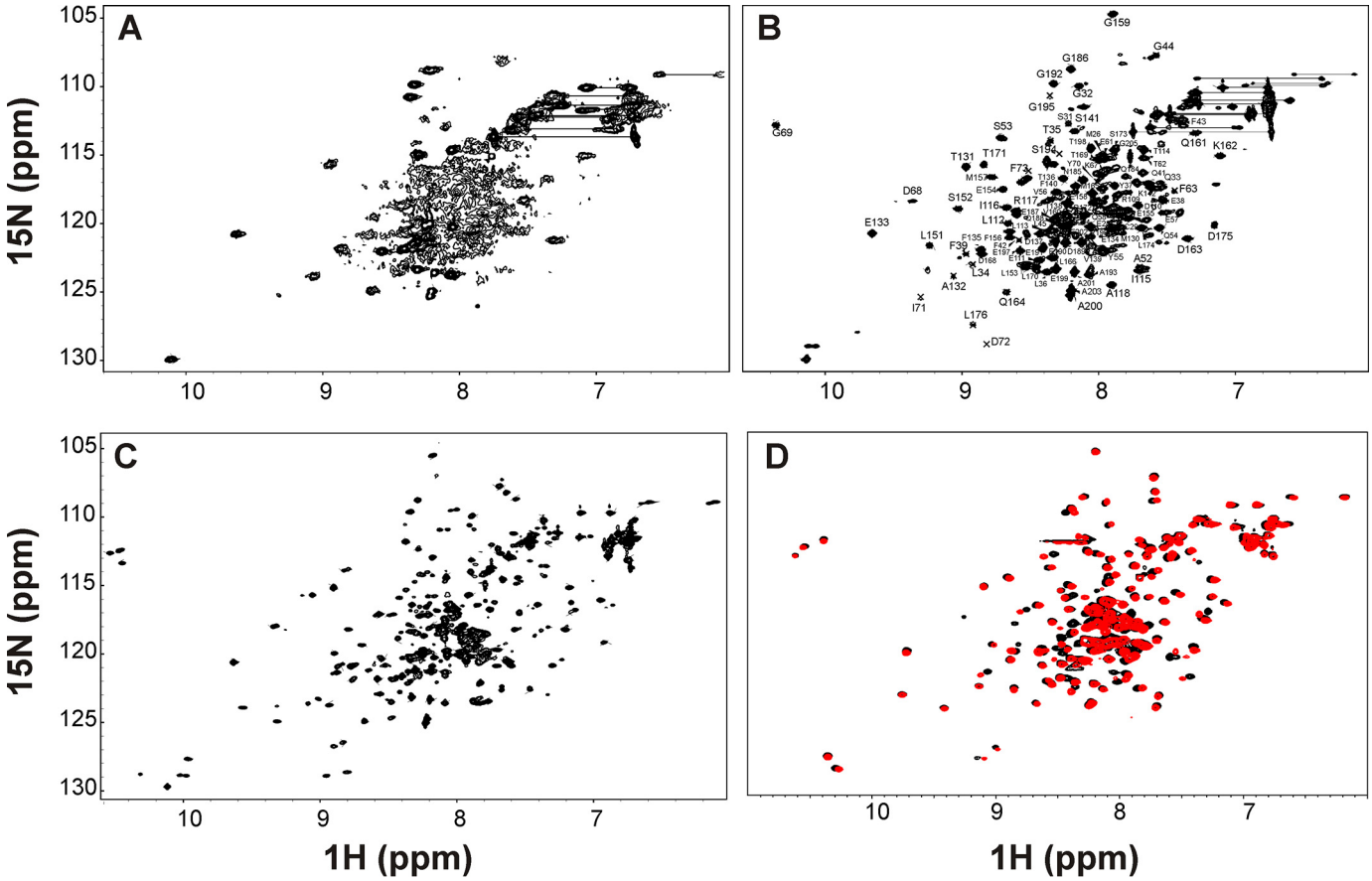

FIGURE 3. **NMR spectroscopy of $GCAP1^{WT}$, $GCAP1^{V77E}$, and mutants (SGL and ΔLeu-174).** Two-dimensional (^1H,^{15}N HSQC) NMR spectra of ^{15}N-labeled wild type GCAP1 in the Ca^{2+}-free/Mg^{2+}-bound state (*A*), $GCAP1^{V77E}$ in the Ca^{2+}-free/Mg^{2+}-bound state (*B*), $GCAP1^{V77E}$ in the Ca^{2+}-bound state (*C*), and GCAP1 mutants (SGL, *black*; ΔLeu-174, *red*) in the Ca^{2+}-bound state (*D*). Spectra were obtained at 37 °C. A downfield resonance at ~10.5 ppm for Ca^{2+}-free/Mg^{2+}-bound $GCAP1^{V77E}$ is assigned to a conserved glycine residue (Gly-69) in EF2 and indicates Mg^{2+} is bound at EF2. Downfield resonances (at 10.45, 10.47, and 10.55 ppm) for Ca^{2+}-bound $GCAP1^{V77E}$ are assigned to conserved glycine residues (Gly-105, Gly-69, and G149) and indicate that three Ca^{2+} are bound per protein at EF2, EF3, and EF4. Sequence-specific resonance assignments for Ca^{2+}-free/Mg^{2+}-bound V77E are indicated by the peak labels. Complete NMR assignments were deposited in the BMRB (accession no. 26688).

structural model of Ca^{2+}-free/Mg^{2+}-bound $GCAP1^{V77E}$ (PDB ID 2NA0) was validated with PROCHECK: 86% of residues belonged to the most favorable region in the Ramachandran plot.

The NMR-derived structural model of Ca^{2+}-free/Mg^{2+}-bound $GCAP1^{V77E}$ (Fig. 5) contains a total of 11 α-helices and 4 β-strands: α1 (residues 7–14), α2 (18–28), α3 (36–43), α4 (51–63), α5 (73–83), α6 (90–99), α7 (109–119), α8 (132–143), α9 (153–161), α10 (164–174), α11 (176–183), β1 (33–35), β2 (70–72), β3 (106–108), and β4 (150–152). $GCAP1^{V77E}$ contains two separate domains comprising four EF hands: EF1 (*green*, residues 18–43) and EF2 (red, residues 51–83) form the N-terminal domain; EF3 (*cyan*, residues 90–119) and EF4 (*yellow*, residues 132–161) form the C-terminal domain. Two C-terminal helices are downstream of EF4 (α10 and α11 in Fig. 4). The helix immediately adjacent to EF4 (α10, *highlighted in orange* in Fig. 5*B*) is one-half turn longer in Ca^{2+}-free/Mg^{2+}-bound $GCAP1^{V77E}$ compared with that of Ca^{2+}-bound GCAP1 (Fig. 6). The C-terminal helix (α11) has the same length in both Ca^{2+}-free and Ca^{2+}-bound GCAP1 and makes contacts with the N-terminal myristoyl group (Fig. 5).

$GCAP1^{V77E}$ contains Mg^{2+} bound at EF2 (*blue sphere* in Fig. 5) as evidenced by characteristic Mg^{2+}-dependent amide chemical shift changes assigned to Gly-69 in EF2 (Fig. 2*A*, *inset*). The geometry of the coordinate covalent bonds formed between chelating amino acid residues in $GCAP1^{V77E}$ and the bound Mg^{2+} could not be observed directly in our NMR study. Instead, the stereochemical geometry and chelation of Mg^{2+} bound at EF2 was modeled with structural constraints derived from the x-ray crystal structure of Mg^{2+}-bound CaM (41), which closely resembles the Mg^{2+} binding site geometry conserved in other EF-hand proteins such as CaBP1 (35) and CaBP4 (31). GCAP1 residues at the 1, 3, and 5 positions of the EF-hand loop in EF2 were selected to chelate the bound Mg^{2+} (see *D64* and *D68* in Fig. 5*A*). Replacement of these two residues disrupted Mg^{2+} binding in our previous biochemical studies (19).

The four EF-hands of $GCAP1^{V77E}$ with one Mg^{2+} bound at EF2 (and no metal bound at EF1, EF3, and EF4) each adopt interhelical angles that are similar to those observed in the crystal structure of Ca^{2+}-bound GCAP1 (Table 2). For the Ca^{2+}-free/Mg^{2+}-bound $GCAP1^{V77E}$ structure, the interhelical angles are 132° (EF1), 114° (EF2), 103° (EF3), and 106° (EF4). Therefore, the three functional EF-hands in GCAP1 (EF2, EF3, and EF4) each adopt a somewhat open conformation in the Ca^{2+}-free state, and Ca^{2+} binding at these sites in

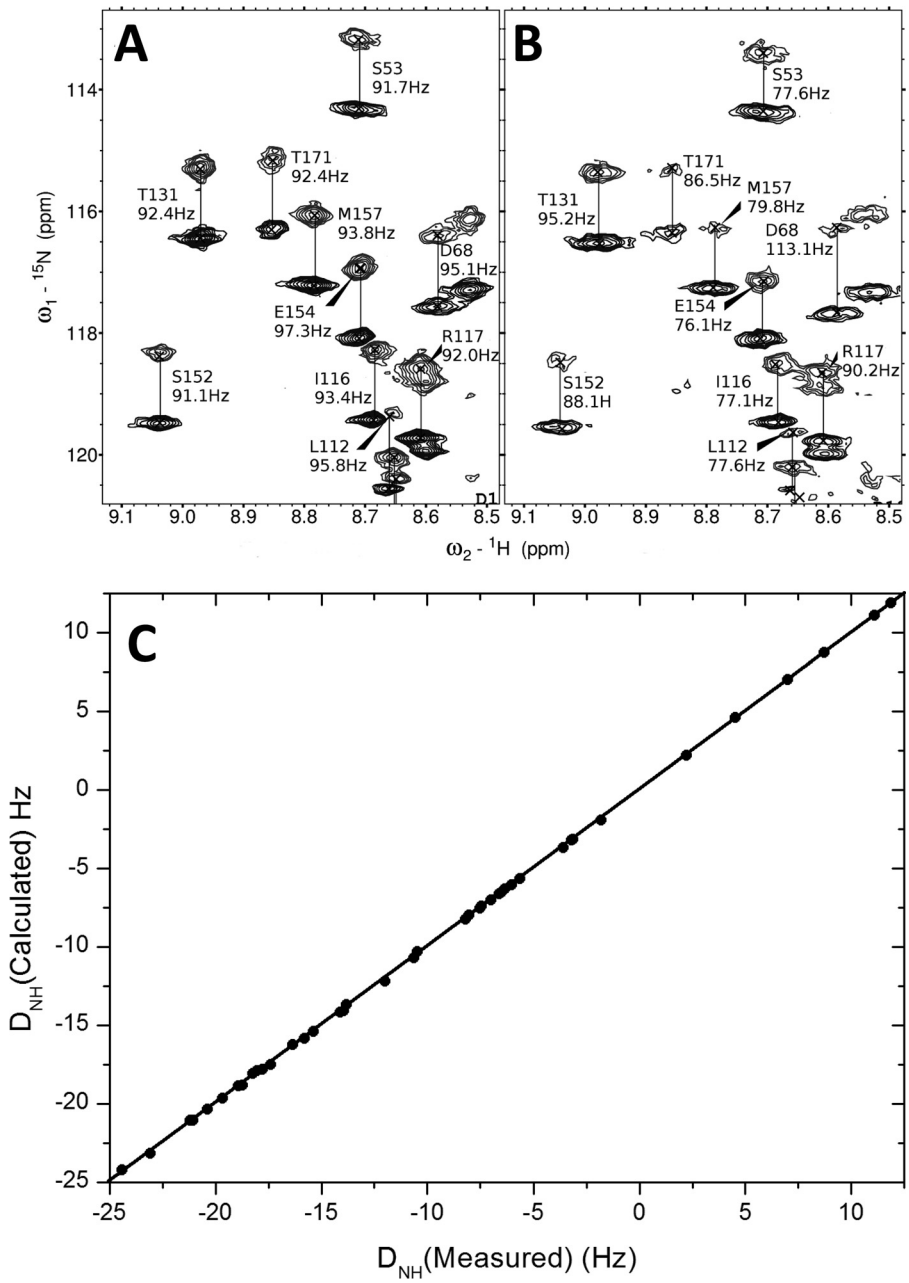

FIGURE 4. **RDC structural analysis of GCAP1^{V77E}.** ^{1}H,^{15}N IPAP (inphase/antiphase)-HSQC spectra of Ca^{2+}-free/Mg^{2+}-bound GCAP1^{V77E} in the absence (*A*) and presence (*B*) of 12 mg/ml Pf1 phage. Spectral splittings for the isotropic condition (J_{NH}) *versus* the anisotropic condition ($J_{NH} + D_{NH}$) are marked by *vertical lines* and were used to calculate RDCs as described under "Experimental Procedures." *C*, RDCs calculated from the structure of Ca^{2+}-free/Mg^{2+}-bound GCAP1^{V77E} in Fig. 5 are plotted *versus* the RDCs measured in Fig. 4*B* and show good agreement (Q-factor = 0.28 and an R-factor = 0.95 (40)).

GCAP1 cause only a slight change in interhelical angle. In essence, the three functional EF-hands in GCAP1 adopt a "pre-formed" open conformation in the Ca^{2+}-free state akin to that of calbindin D_{9k} (42) and other Ca^{2+} buffer proteins (43). As a result, the Ca^{2+}-binding free energy for GCAP1 is NOT coupled to an unfavorable conformational change, which may explain the very high nanomolar Ca^{2+} binding affinity for GCAP1 (25). By stark contrast, myristoylated recoverin (that undergoes a Ca^{2+}-myristoyl switch (44)) and CaM (that undergoes an open-to-closed transition (43)) both bind Ca^{2+} with ~100-fold lower affinity compared with myristoylated GCAP1 (25).

Ca^{2+}-induced Conformational Changes in GCAP1—Chemical shift differences in GCAP1 *versus* Ca^{2+} were plotted as a function of residue number and reveal the location of Ca^{2+}-dependent structural changes (Fig. 6*A*). Detectable chemical shift differences are seen for residues in EF1 (residues 26, 27, and 33) that are implicated in RetGC1 binding (36). Somewhat larger chemical shift changes are seen in EF2 (residues 55, 62, and 68), which represent residues at the domain interface and suggest Ca^{2+}-dependent structural contacts between EF2 and EF3 like that seen previously for recoverin (38, 45). The largest chemical shift differences (highlighted in *red* in Fig. 6*B*) are observed in EF4 (residues 140, 151–152, and 160) and helix α10 (residues

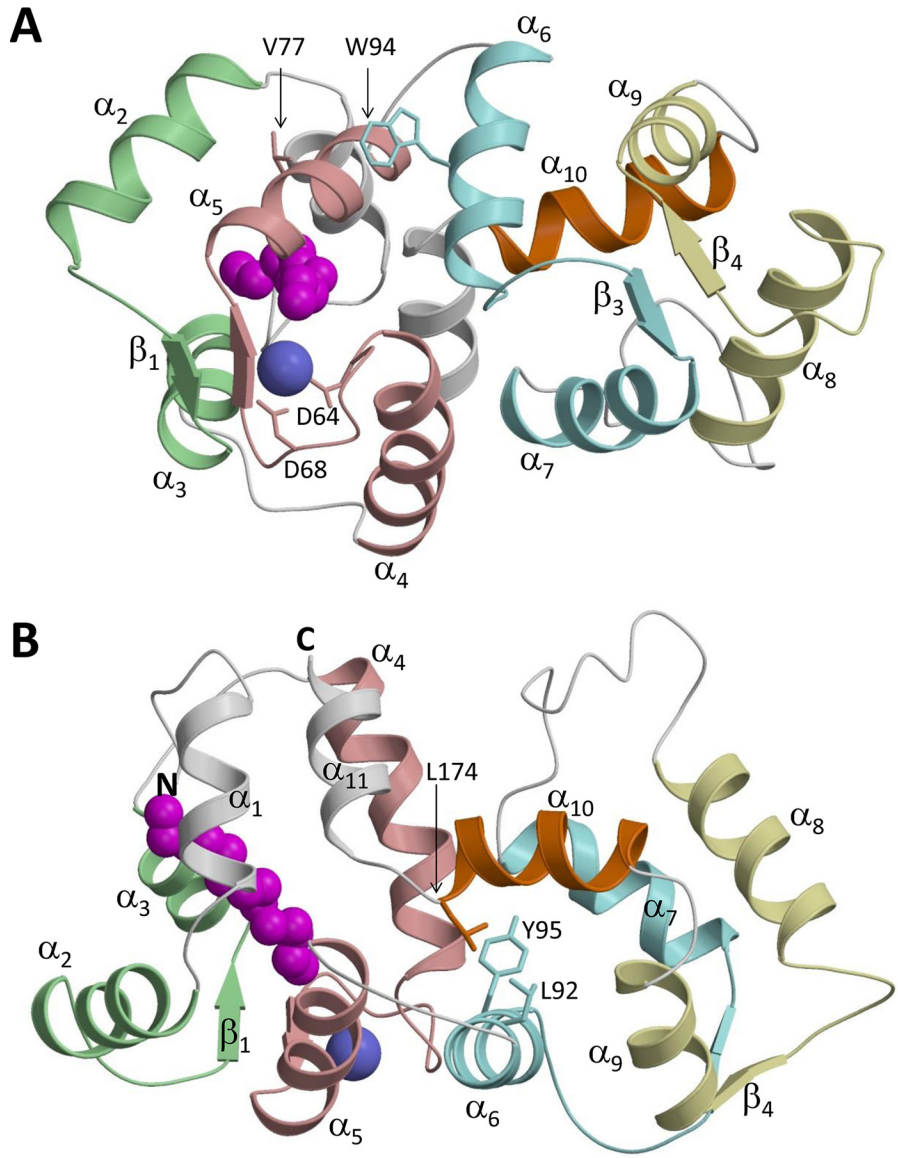

FIGURE 5. **NMR-derived structure of Ca^{2+}-free/Mg^{2+}-bound GCAP1^{V77E} (PDB ID 2NA0).** The main chain structure of Ca^{2+}-free/Mg^{2+}-bound GCAP1^{V77E} (*A*) and the same view rotated by 180 degrees (*B*) show four EF-hands (colored as in Fig. 1) packed in a globular arrangement very similar to what is seen for Ca^{2+}-bound GCAP1 (20). The secondary structural elements are labeled as defined in Fig. 1. The Ca^{2+} switch helix (α10) is highlighted in *orange*, bound Mg^{2+} is in *blue*, and the N-terminal myristoyl group is in *magenta*.

168, 170, and 171), called the Ca^{2+} switch helix. Thus, Ca^{2+}-induced structural changes in EF4 appear coupled to structural changes in the adjacent Ca^{2+} switch helix. An overlay of GCAP1 structures in the Ca^{2+}-free *versus* Ca^{2+}-bound states shows overall main chain root mean square deviations of 2.0 Å. The most striking difference is seen in the Ca^{2+} switch helix (*orange* in Figs. 5*B* and 6*C*), which is one-half-turn longer in the Ca^{2+}-free state. An expanded view of the Ca^{2+} switch helix (Fig. 6*C*) reveals two residues (Thr-171 and Leu-174) that are most affected by Ca^{2+}. Thr-171 is exposed in the Ca^{2+}-free structure, whereas it becomes buried and makes contact with Leu-92 in the Ca^{2+}-bound structure. Conversely, Leu-174 is buried and makes contact with Leu-92 in the Ca^{2+}-free structure, but it switches to a solvent-exposed environment in the Ca^{2+}-bound structure. The Ca^{2+}-dependent contacts formed by both Thr-171 and Leu-174 may be important for switching GCAP1 from the Ca^{2+}-free activator to the Ca^{2+}-bound inhibitor states.

Mutations in the Ca^{2+} Switch Helix Affect Metal Binding and Cyclase Activation—The calcium-myristoyl tug hypothesis (23) proposes a structural link between the exiting helix of EF4 and residues that contact the myristoyl group in the N-domain. Ca^{2+}-induced structural changes in EF4 exert a "tug" on downstream C-terminal residues that are in contact with the myristoyl group. These Ca^{2+}-dependent contacts to the myristate are then relayed to the target binding site in the N-domain (36). We hypothesized that the Ca^{2+}-induced shortening of the Ca^{2+} switch helix observed in our structure (Fig. 6) may transmit the tug action that connects Ca^{2+} binding at EF4 with target activation in the N-domain. Therefore, we tested if a change in the length of the Ca^{2+} switch helix by mutagenesis could affect the regulatory properties of GCAP1. We constructed a

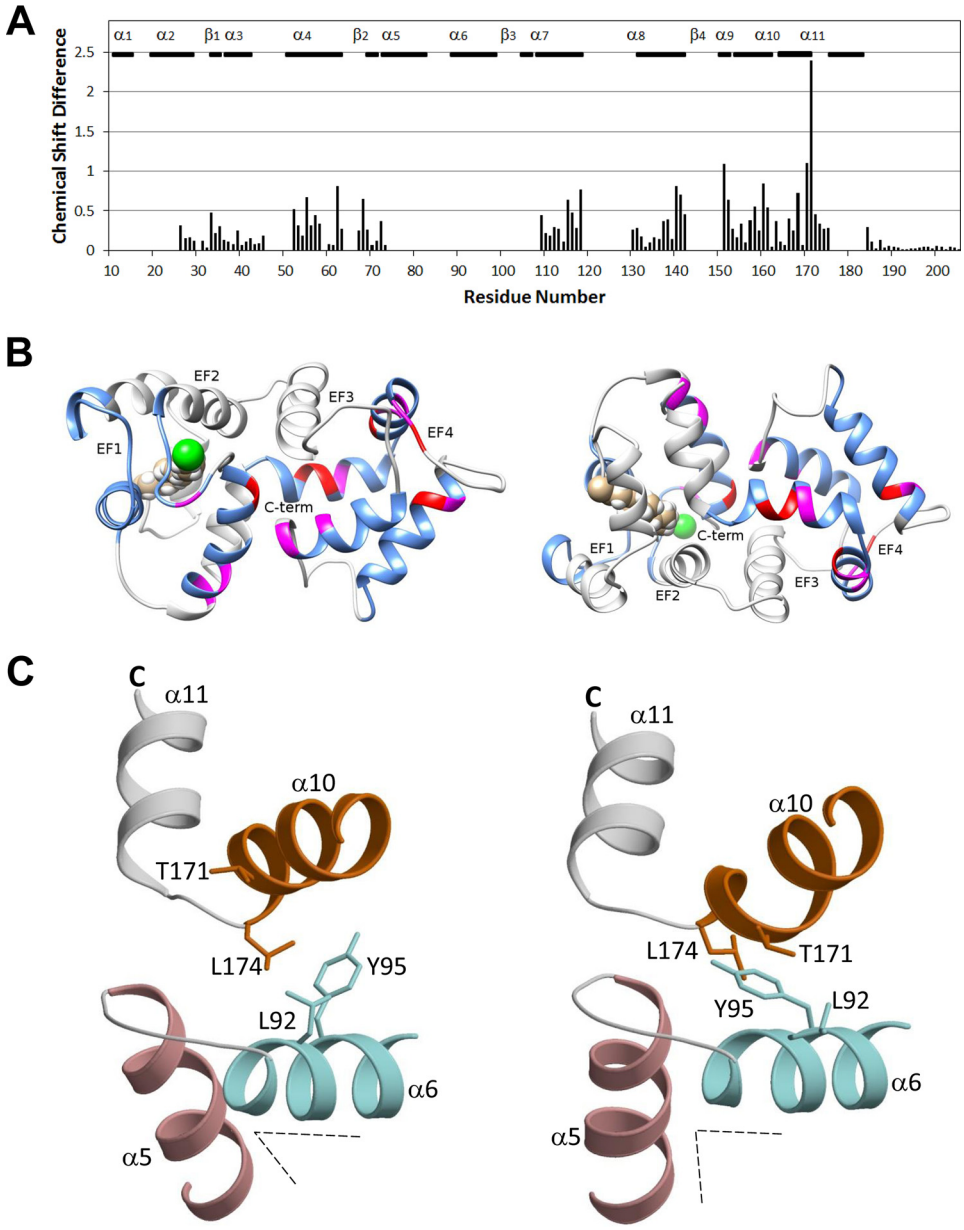

FIGURE 6. **Ca^{2+}-induced conformational changes in GCAP1.** Shown in Ca^{2+}-dependent amide chemical shift difference (Ca^{2+}-free minus Ca^{2+}-bound) plotted *versus* residue number (*A*) and chemical shift difference mapped onto the main chain structure (*B*). Residues Thr-171 and Leu-174 exhibited the largest Ca^{2+}-induced chemical shift differences. Residues (Thr-62, Phe-140, Leu-151, Val-160, Leu-170, Thr-171, Leu-174) with a chemical shift difference higher than 0.8 are colored *red*. Residues (Ala-52, Tyr-55, Asp-68, Ile-115, Ala-118, Ser-141, Ser-152, Glu-158, Gln-161, Asp-168) with a chemical shift difference between 0.5 and 0.8 are colored *magenta*. Residues with a chemical shift difference <0.5 are colored light *blue*. *C*, close-up view of the Ca^{2+} switch helix (α10, *orange*) that is elongated by one turn in Ca^{2+}-free/Mg^{2+}-bound $GCAP1^{V77E}$ (*left*) compared with Ca^{2+}-bound $GCAP1^{WT}$ (*right*). The angle between EF2 exiting helix (*red*) and EF3 entering helix (*cyan*) at the domain interface increased slightly (*dotted line*) due to Ca^{2+}-dependent interactions with the Ca^{2+} switch helix.

series of mutants in which the length of the helix was altered either by insertion or deletion of a single amino acid: a Gly was inserted between Ser-173 and Leu-174 (SGL mutant, Fig. 7), and single amino acids were deleted: Arg-172 (ΔArg-172), Ser-173 (ΔSer-173), or Leu-174 (ΔLeu-174) (Fig. 8). NMR HSQC spectra demonstrate that these mutations do not alter the conformation of α10 and these mutants are structurally intact (Fig. 3*D*). We found that each of these mutants (which changes the length of the Ca^{2+} switch helix) profoundly affected both the metal binding affinity of GCAP1 and its ability to activate RetGC. The Ca^{2+} binding stoichiometry in the SGL mutant remained three per GCAP1 molecule, but the apparent affinity decreased slightly with higher cooperativity compared with that of wild type (Fig. 6A). Metal-dependent changes in the intrinsic Trp fluorescence of the SGL mutant looked quite different from that of wild type (Fig. 7, *B–D*). The Ca^{2+}-induced decrease in fluorescence (in the absence of Mg^{2+}) occurred at higher Ca^{2+} levels in SGL compared with wild type (Fig. 7*B*). The presence of 10 mM Mg^{2+} (that normally causes a quite striking Ca^{2+}-induced increase in Trp fluorescence for wild type) resulted in much smaller Ca^{2+}-dependent change in Trp fluorescence for SGL (Fig. 7*C*). Thus, the transition from the Mg^{2+}-bound activator state to the Ca^{2+}-bound inhibitor state in the presence of 10 mM Mg^{2+} (19) was more difficult to mon-

TABLE 2
Interhelical angles of the EF-hands in GCAP1 and CaM
Residues in the helices are as shown in the footnotes.

Helix pairs	Interhelical angles			
	ApoCaM[a]	Ca^{2+}-bound CaM[b]	Mg^{2+}-bound GCAP1[c]	Ca^{2+}-bound GCAP1[c]
	Degree			
EF1 (α_1-α_2)	130.9	103.8	132.1	132.7
EF2 (α_3-α_4)	130.8	101.0	113.9	112.1
EF3 (α_5-α_6)	139.5	101.0	102.9	103.1
EF4 (α_7-α_8)	126.0	101.0	106.1	104.0

[a] ApoCaM (PDB accession code 1DMO): (α1) 6–18, (α2) 29–38, (α3) 45–55, (α4) 65–75, (α5) 82–90, (α6) 103–112, (α7)118–127, (α8) 137–143.
[b] Ca^{2+}-bound CaM (PDB accession code 1J7P): (α1) 6–19, (α2) 29–38, (α3) 45–55, (α4) 65–75, (α5) 83–92, (α6) 102–111, (α7)118–128, (α8) 138–145.
[c] GCAP1: (α_1) 18–27, (α_2) 36–43, (α_3) 51–63, (α_4) 73–82, (α_5) 90–99, (α_6) 109–119, (α_7) 132–143, (α_8) 153–161.

itor in SGL compared with wild type (Fig. 7*C*). In addition, the Trp fluorescence of the SGL mutant titrated as a function of Mg^{2+} revealed a nearly 10-fold lower Mg^{2+} binding affinity compared with that of wild type (Fig. 7*D*). Because Mg^{2+} binding to EF2 is essential for converting GCAP1 into its activated state in the absence of Ca^{2+} (10, 19), we tested if RetGC1 activation was also affected by this mutation. Indeed, the SGL mutant failed to activate RetGC1 at physiological concentrations of Mg^{2+} and when the Ca^{2+} concentration was reduced to levels typical of light-exposed photoreceptors (Fig. 7*D*).

Making the Ca^{2+} switch helix shorter by a single residue produced a similar effect regardless of which amino acid was deleted, Arg-172, Ser-173, or Leu-174 (Fig. 8). In all three deletion mutants, the Ca^{2+}-induced decrease in Trp fluorescence looked similar to that of wild type (Fig. 8, *A–C*, *red symbols*), except for a slight 2-fold shift toward higher Ca^{2+} concentrations (Fig. 8*D*). As seen above for SGL, the presence of 10 mM Mg^{2+} caused a much smaller change in Ca^{2+}-dependent Trp fluorescence for each of the deletion mutants, thus making it difficult to monitor the transition from the Mg^{2+}-bound activator state to the Ca^{2+}-bound inhibitor state (Fig. 8, *A–C*, *blue symbols*) in contrast to the much larger Ca^{2+}-induced fluorescence change seen for wild type (Fig. 7*B*). As seen above for SGL, the Trp fluorescence of the deletion mutants titrated as a function of Mg^{2+} revealed a nearly 10-fold lower Mg^{2+} binding affinity compared with that of wild type (Fig. 8*E*). Finally, the deletion mutants all failed to activate RetGC1 at physiological concentrations of Mg^{2+}, consistent with their lack of Mg^{2+} binding (Fig. 8*F*).

Discussion

NCS proteins like recoverin and NCS-1 undergo large Ca^{2+}-induced conformational changes that cause extrusion of the N-terminal myristoyl group, termed Ca^{2+}-myristoyl switch (38, 46–48). Surprisingly, the GCAP proteins do not possess a Ca^{2+}-myristoyl switch (17, 49, 50), and the N-terminal myristoyl group remains buried inside the protein in both Ca^{2+}-free and Ca^{2+}-bound GCAPs (17, 51). Although NMR and crystal structures are known for Ca^{2+}-bound GCAPs (20–22, 52), before this study little was known structurally about the Mg^{2+}-bound/Ca^{2+}-free activator state of GCAPs and how Ca^{2+}-induced conformational changes in GCAPs control cyclase activation.

In this study we present NMR assignments (Fig. 3*B*), NOEs (Table 1), RDCs (Fig. 4), and mutagenesis data (Fig. 7) to probe Ca^{2+}-dependent conformational changes between the Ca^{2+}-saturated inhibitory state *versus* the Ca^{2+}-free/Mg^{2+}-bound $GCAP1^{V77E}$ (Fig. 6). Overall, the NMR chemical shift differences between Ca^{2+}-saturated wild type GCAP1 and Ca^{2+}-free/Mg^{2+}-bound $GCAP1^{V77E}$ are relatively small (Fig. 6*A*), consistent with an overall similar main chain conformation for the two states (root mean square deviations = 2.0 Å). This contrasts with the large Ca^{2+}-induced conformational changes seen for other EF-hand proteins, including recoverin (38), NCS-1 (48), CaM (53, 54), and troponin-C (55). The large Ca^{2+}-induced conformational changes in recoverin and CaM both drive the exposure of hydrophobic residues, which consumes Ca^{2+} binding free energy and accounts for their low binding affinity. The Ca^{2+}-free EF-hands in GCAP1 adopt a preformed open conformation, like what is seen for calbindin D9k (42) and other Ca^{2+} buffer proteins (43). The lack of any large scale Ca^{2+}-induced protein conformational change in GCAP1, therefore, may explain why the GCAPs bind Ca^{2+} with at least 100-fold higher affinity compared with that of recoverin (44) and CaM.

The most apparent Ca^{2+}-induced structural changes in GCAP1 are localized in EF4 and the adjacent Ca^{2+} switch helix (α10). Ca^{2+} binding to EF4 is essential for switching GCAP1 between activator and inhibitor states (10, 19). Upon Ca^{2+} binding to EF4, its interhelical angle decreases by 2° (Table 2) along with a slight lengthening of the exiting helix (α9) that in turn exerts a force (tug) on the adjacent Ca^{2+} switch helix (α10). As a result, the Ca^{2+} switch helix is one half-turn longer in the Ca^{2+}-free structure compared with the Ca^{2+}-bound structure (Fig. 6, *B* and *C*). The Ca^{2+}-induced shortening of the Ca^{2+} switch helix alters the disposition of key residues (Thr-171 and Leu-174) that form Ca^{2+}-dependent contacts with EF3 (Leu-92 and Tyr-95). These Ca^{2+}-dependent contacts alter the packing angle between helices α5 and α6 at the domain interface (Fig. 6*C*) that resembles the Ca^{2+}-induced domain swiveling in recoverin (38). The Ca^{2+}-dependent structural changes in the Ca^{2+} switch helix also exert a force on the C-terminal helix (α11) that alters its contact with the myristoyl group. We propose that this Ca^{2+}-dependent perturbation of the myristoyl group could alter its contact with EF1 and EF2 and thereby affect the accessibility of GCAP1 residues (Met-26, Tyr-37, Val-77, and Ala-78) in the RetGC1 binding site (36). In essence, the Ca^{2+}-induced structural changes in EF4 are relayed to the cyclase binding site via the Ca^{2+} switch helix. This relay scheme is consistent with a previously proposed mechanism called the Ca^{2+}-myristoyl tug (23).

We further find here that even though the Ca^{2+} switch helix (α10) is not an immediate part of the RetGC binding interface (36), the length of α10 critically affects proper binding of Ca^{2+} (23) and Mg^{2+} (Figs. 7 and 8). This effect on Mg^{2+} binding (Figs. 7 and 8) is especially important for the RetGC1 binding site in GCAP1, which includes the N-domain and requires Mg^{2+} binding in EF2 to interact with the cyclase at low Ca^{2+} levels that occur in light-adapted photoreceptors (19, 36, 56). Evidently, the length of the Ca^{2+} switch helix (α10) in wild type GCAP1 has evolved to optimize the proper tug action between

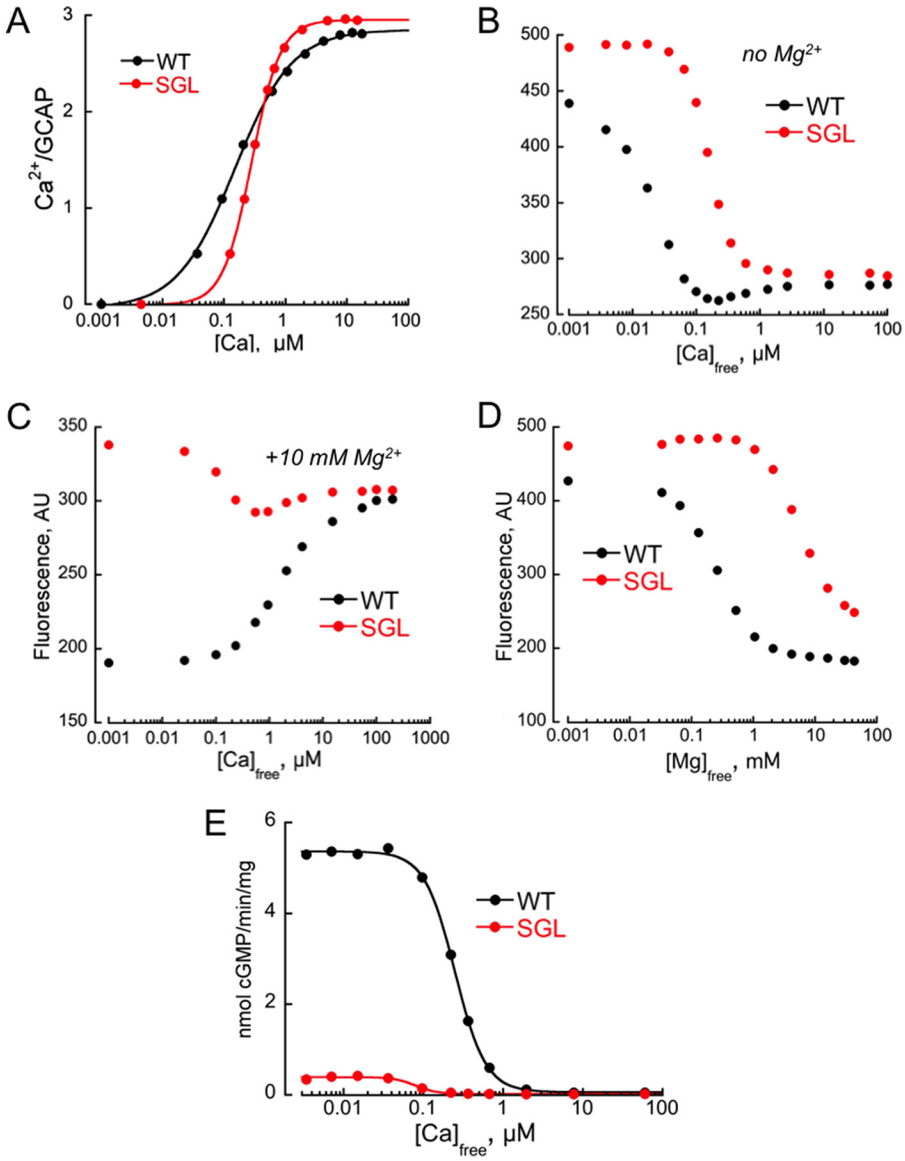

FIGURE 7. **Single amino acid residue insertion in the Ca^{2+} switch helix affects metal sensor properties of GCAP1.** *A*, Ca^{2+} binding isotherm for wild type (*black*, ●) and SGL (*red*, ●) GCAP1. Ca^{2+} binding was assayed using titration of 20 μM GCAP1 in the presence of Fluo4FF as described under "Experimental Procedures." *B–D*, tryptophan fluorescence titrations for monitoring metal-dependent conformational change in wild type (*black*, ●) and SGL (*red*, ●) GCAP1 caused by Ca^{2+} (*B* and *C*) or Mg^{2+} (*D*) binding. *B* and *C*, Ca^{2+} titration in the absence (*B*) or in the presence (*C*) of 10 mM Mg^{2+}. *AU*, absorbance units. *D*, Mg^{2+} titration. *E*, RetGC1 activation *in vitro* by wild type (*black*, ●) and SGL (*red*, ●) GCAP1 in the presence of 1 mM Mg^{2+} was assayed as described under "Experimental Procedures."

the N- and C-domains, which tunes the Ca^{2+} and especially Mg^{2+} binding affinity into the physiological range.

GCAP1 residues in EF2 and EF3 located at the domain interface (Val-77–Trp-94, see Figs. 1 and 6) exhibit exchange-broadened NMR resonances and are conformationally dynamic. The dynamical nature of these residues is consistent with Ca^{2+}-induced conformational changes in GCAP1 at the domain interface that were observed previously (13, 57). The corresponding residues in recoverin (Fig. 1) also exhibited broad NMR resonances, and ^{15}N NMR relaxation dispersion studies revealed that these residues at the domain interface exhibit backbone dynamics on the millisecond timescale (45). Ca^{2+}-induced rearrangement of residues at the domain interface in recoverin gives rise to a 45-degree swiveling of the two domains (38). Our structural model of Mg^{2+}-bound/Ca^{2+}-free $GCAP1^{V77E}$ suggests a related but smaller Ca^{2+}-induced rearrangement at the domain interface (Fig. 6). Residues Tyr-55, Thr-62, and Ala-118 at the domain interface exhibit large Ca^{2+}-induced chemical shift differences (Fig. 6*A*). In addition, residues in EF3 (Leu-92 and Tyr-95) make Ca^{2+}-dependent contacts with Thr-171 and Leu-174 in the Ca^{2+} switch helix (Fig. 6*C*). These Ca^{2+}-dependent contacts to EF3 cause a change in packing angle between EF2 and EF3 at the domain interface (see the *dotted line* in Fig. 6*C*) that is somewhat reminiscent of the Ca^{2+}-dependent domain swiveling observed for recoverin (38, 45).

NMR relaxation data and size-exclusion chromatography analysis previously showed that GCAP1 is dimeric in solution at high micromolar protein concentration (22). A GCAP1 homolog, GCAP2, undergoes a Ca^{2+}-sensitive dimerization at low

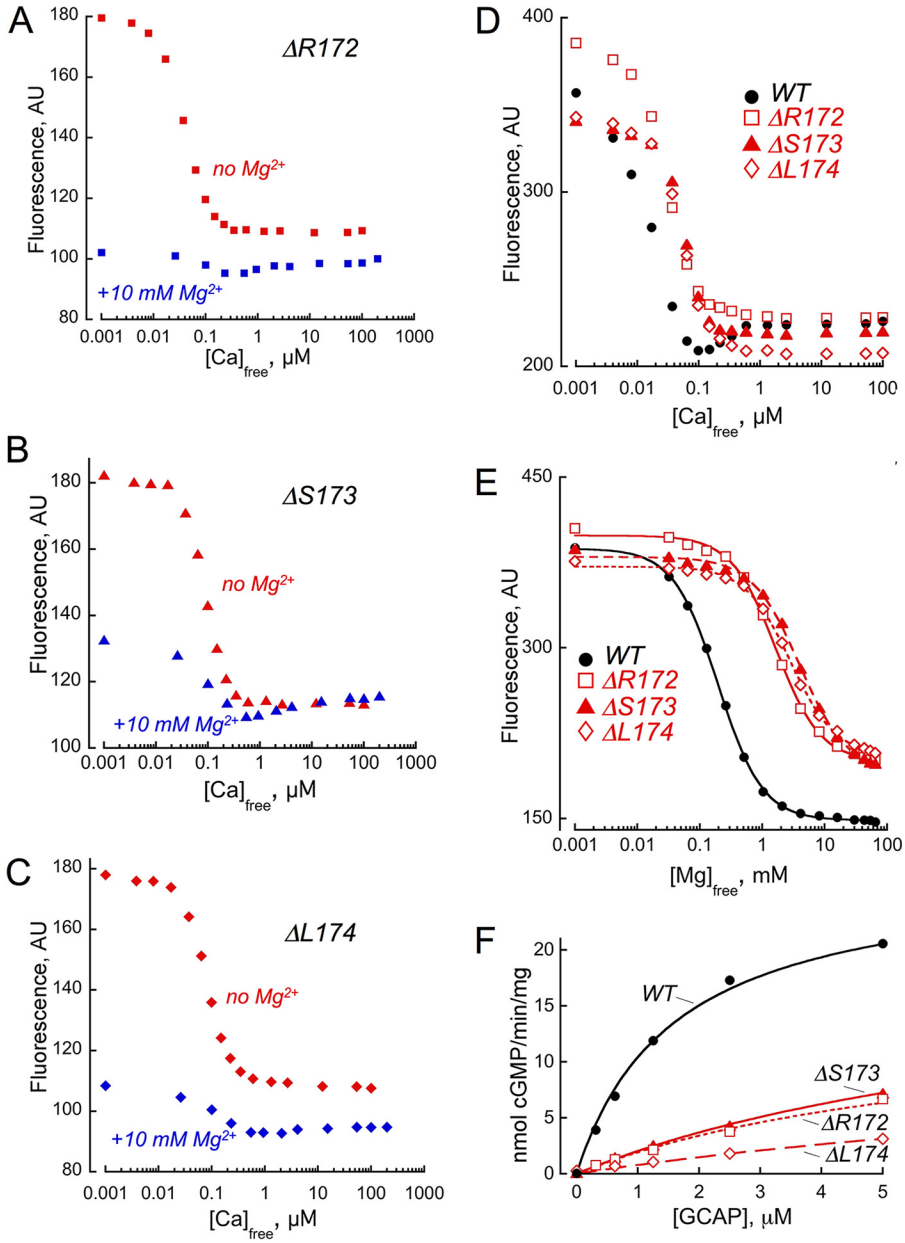

FIGURE 8. **Effect of a single amino acid residue deletion in Ca^{2+} switch helix on metal sensor properties of GCAP1.** *A–C*, tryptophan fluorescence titrations for monitoring Ca^{2+}-dependent conformational change in ΔArg-172 (■) (*A*), ΔSer-173 (▲) (*B*), or ΔLeu-174 (♦) (*C*) GCAP1 in the absence (*red symbols*) or in the presence (*blue symbols*) of 10 mM Mg^{2+}. *AU*, absorbance units. *D* and *E*, comparison of the Ca^{2+}-dependent (*D*) or Mg^{2+}-dependent (*E*) Trp fluorescence change in the wild type (*black*, ●), ΔArg-172 (□) (*A*), ΔSer-173 (▲) (*B*), or ΔLeu-174 (◇); no Mg^{2+} added in *D*. *F*, dose dependence of RetGC1 activation *in vitro* by wild type (*black*, ●) ΔArg-172 (*red*, □), ΔSer-173 (*red*, ▲), or ΔLeu-174 (red ◇) GCAP1 in the presence of 6 mM free Mg^{2+} and 2 mM EGTA; the data points were fitted using Synergy Kaleidagraph 4 software assuming a standard Michaelis hyperbolic function.

micromolar protein concentrations, which originally suggested that reversible dimerization may control formation and activation of RetGC:GCAP in a 2:2 complex (58, 59). Although dimerization of GCAP1 observed by Lim *et al.* (22) does not appear to be Ca^{2+}-sensitive, it is possible that GCAP1 dimerization might promote a functional interaction within a RetGC1 dimer on the disk membrane (60, 61). The binding stoichiometry of the GCAP1:RetGC1 complex has been estimated to be equimolar (62), consistent with a 2:2 complex that contains a RetGC1 dimer bound to a GCAP1 dimer. Previously we showed that the V77E mutation in GCAP1 eliminated GCAP1 dimerization and abolished its ability to bind RetGC but did not block its ability to undergo the functional transition between Ca^{2+}-bound and Mg^{2+}-bound states (22, 36). If GCAP1 dimerization is important for RetGC activation, allosteric changes in the GCAP1 dimer quaternary structure may control cyclase activation. In this scenario a small Ca^{2+}-induced change in tertiary structure could lead to a much larger change in quaternary structure akin to the O_2-dependent conformational changes in hemoglobin (63). Hydrophobic residues at the GCAP1 domain interface (Val-77, Ala-78, Leu-82, Trp-94) are solvent-exposed and might mediate specific contacts that control RetGC1 binding and GCAP1 dimerization alike. However, it cannot be excluded that these exposed GCAP1 res-

idues may create an artificial dimer at high concentrations and in the absence of the target enzyme. Future studies are needed to further probe the dimeric structure of GCAP1 and determine whether Ca^{2+}-induced changes in quaternary structure might control its activation of RetGC1.

Author Contributions—J. B. A. directed the overall project and wrote the paper. S. L. performed NMR and ITC experiments, analyzed the NMR and ITC data, performed structure calculations, and helped write the manuscript. E. V. O. and A. M. D. constructed the mutants. I. V. P. assayed Trp fluorescence, Ca^{2+} binding stoichiometry, and RETGC activity. I. V. P. and A. M. D. analyzed the mutagenesis data and participated in writing the manuscript.

Acknowledgments—We thank Jeff Walton and Bennett Addison for technical support and help with NMR experiments.

References

1. Ames, J. B., Tanaka, T., Stryer, L., and Ikura, M. (1996) Portrait of a myristoyl switch protein. *Curr. Opin. Struct. Biol.* **6,** 432–438
2. Burgoyne, R. D. (2007) Neuronal calcium sensor proteins: generating diversity in neuronal Ca^{2+} signalling. *Nat. Rev. Neurosci.* **8,** 182–193
3. Burgoyne, R. D., and Weiss, J. L. (2001) The neuronal calcium sensor family of Ca^{2+}-binding proteins. *Biochem. J.* **353,** 1–12
4. Dizhoor, A. M., Lowe, D. G., Olshevskaya, E. V., Laura, R. P., and Hurley, J. B. (1994) The human photoreceptor membrane guanylyl cyclase, RetGC, is present in outer segments and is regulated by calcium and a soluble activator. *Neuron* **12,** 1345–1352
5. Koch, K. W., and Stryer, L. (1988) Highly cooperative feedback control of retinal rod guanylate cyclase by calcium ions. *Nature* **334,** 64–66
6. Palczewski, K., Subbaraya, I., Gorczyca, W. A., Helekar, B. S., Ruiz, C. C., Ohguro, H., Huang, J., Zhao, X., Crabb, J. W., and Johnson, R. S. (1994) Molecular cloning and characterization of retinal photoreceptor guanylyl cyclase-activating protein. *Neuron* **13,** 395–404
7. Palczewski, K., Polans, A. S., Baehr, W., and Ames, J. B. (2000) Ca^{2+}-binding proteins in the retina: structure, function, and the etiology of human visual diseases. *Bioessays* **22,** 337–350
8. Stephen, R., Filipek, S., Palczewski, K., and Sousa, M. C. (2008) Ca^{2+}-dependent regulation of phototransduction. *Photochem. Photobiol.* **84,** 903–910
9. Payne, A. M., Downes, S. M., Bessant, D. A., Taylor, R., Holder, G. E., Warren, M. J., Bird, A. C., and Bhattacharya, S. S. (1998) A mutation in guanylate cyclase activator 1A (GUCA1A) in an autosomal dominant cone dystrophy pedigree mapping to a new locus on chromosome 6p21.1. *Hum. Mol. Genet.* **7,** 273–277
10. Peshenko, I. V., and Dizhoor, A. M. (2007) Activation and inhibition of photoreceptor guanylyl cyclase by guanylyl cyclase activating protein 1 (GCAP-1): the functional role of Mg^{2+}/Ca^{2+} exchange in EF-hand domains. *J. Biol. Chem.* **282,** 21645–21652
11. Dizhoor, A. M., and Hurley, J. B. (1996) Inactivation of EF-hands makes GCAP-2 (p24) a constitutive activator of photoreceptor guanylyl cyclase by preventing a Ca^{2+}-induced "activator-to-inhibitor" transition. *J. Biol. Chem.* **271,** 19346–19350
12. Hwang, J. Y., and Koch, K. W. (2002) Calcium- and myristoyl-dependent properties of guanylate cyclase-activating protein-1 and protein-2. *Biochemistry* **41,** 13021–13028
13. Krylov, D. M., Niemi, G. A., Dizhoor, A. M., and Hurley, J. B. (1999) Mapping sites in guanylyl cyclase activating protein-1 required for regulation of photoreceptor membrane guanylyl cyclases. *J. Biol. Chem.* **274,** 10833–10839
14. Dizhoor, A. M., Olshevskaya, E. V., Henzel, W. J., Wong, S. C., Stults, J. T., Ankoudinova, I., and Hurley, J. B. (1995) Cloning, sequencing, and expression of a 24-kDa Ca^{2+}-binding protein activating photoreceptor guanylyl cyclase. *J. Biol. Chem.* **270,** 25200–25206
15. Imanishi, Y., Li, N., Sokal, I., Sowa, M. E., Lichtarge, O., Wensel, T. G., Saperstein, D. A., Baehr, W., and Palczewski, K. (2002) Characterization of retinal guanylate cyclase-activating protein 3 (GCAP3) from zebrafish to man. *Eur. J. Neurosci.* **15,** 63–78
16. Imanishi, Y., Yang, L., Sokal, I., Filipek, S., Palczewski, K., and Baehr, W. (2004) Diversity of guanylate cyclase-activating proteins (GCAPs) in teleost fish: characterization of three novel GCAPs (GCAP4, GCAP5, GCAP7) from zebrafish (Danio rerio) and prediction of eight GCAPs (GCAP1–8) in pufferfish (Fugu rubripes). *J. Mol. Evol.* **59,** 204–217
17. Lim, S., Peshenko, I., Dizhoor, A., and Ames, J. B. (2009) Effects of Ca^{2+}, Mg^{2+}, and myristoylation on guanylyl cyclase activating protein 1 structure and stability. *Biochemistry* **48,** 850–862
18. Olshevskaya, E. V., Peshenko, I. V., Savchenko, A. B., and Dizhoor, A. M. (2012) Retinal guanylyl cyclase isozyme 1 is the preferential *in vivo* target for constitutively active GCAP1 mutants causing congenital degeneration of photoreceptors. *J. Neurosci.* **32,** 7208–7217
19. Peshenko, I. V., and Dizhoor, A. M. (2006) Ca^{2+} and Mg^{2+} binding properties of GCAP-1: evidence that Mg^{2+}-bound form is the physiological activator of photoreceptor guanylyl cyclase. *J. Biol. Chem.* **281,** 23830–23841
20. Stephen, R., Bereta, G., Golczak, M., Palczewski, K., and Sousa, M. C. (2007) Stabilizing function for myristoyl group revealed by the crystal structure of a neuronal calcium sensor, guanylate cyclase-activating protein 1. *Structure* **15,** 1392–1402
21. Ames, J. B., Dizhoor, A. M., Ikura, M., Palczewski, K., and Stryer, L. (1999) Three-dimensional structure of guanylyl cyclase activating protein-2, a calcium-sensitive modulator of photoreceptor guanylyl cyclases. *J. Biol. Chem.* **274,** 19329–19337
22. Lim, S., Peshenko, I. V., Dizhoor, A. M., and Ames, J. B. (2013) Structural insights for activation of retinal guanylate cyclase by GCAP1. *PLoS ONE* **8,** e81822
23. Peshenko, I. V., Olshevskaya, E. V., Lim, S., Ames, J. B., and Dizhoor, A. M. (2012) Calcium-myristoyl tug. *J. Biol. Chem.* **287,** 13972–13984
24. Olshevskaya, E. V., Calvert, P. D., Woodruff, M. L., Peshenko, I. V., Savchenko, A. B., Makino, C. L., Ho, Y. S., Fain, G. L., and Dizhoor, A. M. (2004) The Y99C mutation in guanylyl cyclase-activating protein 1 increases intracellular Ca^{2+} and causes photoreceptor degeneration in transgenic mice. *J. Neurosci.* **24,** 6078–6085
25. Lim, S., and Ames, J. B. (2009) ^{1}H, ^{15}N, and ^{13}C chemical shift assignments of neuronal calcium sensor-1 homolog from fission yeast. *Biomol. NMR Assign.* **3,** 269–271
26. Ikura, M., Kay, L. E., and Bax, A. (1990) A novel approach for sequential assignment of ^{1}H, ^{13}C, and ^{15}N spectra of proteins: heteronuclear triple-resonance three-dimensional NMR spectroscopy; application to calmodulin. *Biochemistry* **29,** 4659–4667
27. Tjandra, N., and Bax, A. (1997) Direct measurement of disances and angles in biomolecules by NMR in a dilute liquid crystalline medium. *Science* **278,** 1111–1114
28. Delaglio, F., Grzesiek, S., Vuister, G. W., Zhu, G., Pfeifer, J., and Bax, A. (1995) NMRPipe: a multidimensional spectral processing system based on UNIX pipes. *J. Biomol. NMR* **6,** 277–293
29. Badger, J., Kumar, R. A., Yip, P., and Szalma, S. (1999) New features and enhancements in the X-PLOR computer program. *Proteins* **35,** 25–33
30. Schwieters, C. D., Kuszewski, J. J., Tjandra, N., and Clore, G. M. (2003) The Xplor-NIH NMR molecular structure determination package. *J. Magn. Reson.* **160,** 65–73
31. Park, S., Li, C., Haeseleer, F., Palczewski, K., and Ames, J. B. (2014) Structural insights into activation of the retinal L-type Ca^{2+} channel (Cav1.4) by Ca^{2+}-binding protein 4 (CaBP4). *J. Biol. Chem.* **289,** 31262–31273
32. Nilges, M., Gronenborn, A. M., Brünger, A. T., and Clore, G. M. (1988) Determination of three-dimensional structures of proteins by simulated annealing with interproton distance restraints: application to crambin, potato carboxypeptidase inhibitor, and barley serine proteinase inhibitor 2. *Protein Eng.* **2,** 27–38
33. Shen, Y., Delaglio, F., Cornilescu, G., and Bax, A. (2009) TALOS+: a hybrid method for predicting protein backbone torsion angles from NMR chemical shifts. *J. Biomol. NMR* **44,** 213–223
34. Wingard, J. N., Chan, J., Bosanac, I., Haeseleer, F., Palczewski, K., Ikura, M., and Ames, J. B. (2005) Structural analysis of Mg^{2+} and Ca^{2+} binding to

CaBP1, a neuron-specific regulator of calcium channels. *J. Biol. Chem.* **280,** 37461–37470
35. Li, C., Chan, J., Haeseleer, F., Mikoshiba, K., Palczewski, K., Ikura, M., and Ames, J. B. (2009) Structural insights into Ca^{2+}-dependent regulation of inositol 1,4,5-trisphosphate receptors by CaBP1. *J. Biol. Chem.* **284,** 2472–2481
36. Peshenko, I. V., Olshevskaya, E. V., Lim, S., Ames, J. B., and Dizhoor, A. M. (2014) Identification of target binding site in photoreceptor guanylyl cyclase-activating protein 1 (GCAP1). *J. Biol. Chem.* **289,** 10140–10154
37. Lim, S., Peshenko, I. V., Dizhoor, A. M., and Ames, J. B. (2013) Backbone ^{1}H, ^{13}C, and ^{15}N resonance assignments of guanylyl cyclase activating protein-1, GCAP1. *Biomol. NMR Assign.* **7,** 39–42
38. Ames, J. B., Ishima, R., Tanaka, T., Gordon, J. I., Stryer, L., and Ikura, M. (1997) Molecular mechanics of calcium-myristoyl switches. *Nature* **389,** 198–202
39. Tanaka, T., Ames, J. B., Harvey, T. S., Stryer, L., and Ikura, M. (1995) Sequestration of the membrane-targeting myristoyl group of recoverin in the calcium-free state. *Nature* **376,** 444–447
40. Zweckstetter, M. (2008) NMR: prediction of molecular alignment from structure using the PALES software. *Nat. Protoc.* **3,** 679–690
41. Senguen, F. T., and Grabarek, Z. (2012) X-ray structures of magnesium and manganese complexes with the N-terminal domain of calmodulin: insights into the mechanism and specificity of metal ion binding to an EF-hand. *Biochemistry* **51,** 6182–6194
42. Skelton, N. J., Kördel, J., and Chazin, W. J. (1995) Determination of the solution structure of apo calbindin D9k by NMR spectroscopy. *J. Mol. Biol.* **249,** 441–462
43. Ikura, M. (1996) Calcium binding and conformational response in EF-hand proteins. *Trends Biochem. Sci.* **21,** 14–17
44. Ames, J. B., Porumb, T., Tanaka, T., Ikura, M., and Stryer, L. (1995) Amino-terminal myristoylation induces cooperative calcium binding to recoverin. *J. Biol. Chem.* **270,** 4526–4533
45. Xu, X., Ishima, R., and Ames, J. B. (2011) Conformational dynamics of recoverin's Ca^{2+}-myristoyl switch probed by 15N NMR relaxation dispersion and chemical shift analysis. *Proteins* **79,** 1910–1922
46. Ames, J. B., and Lim, S. (2012) Molecular structure and target recognition of neuronal calcium sensor proteins. *Biochim. Biophys. Acta* **1820,** 1205–1213
47. Lim, S., Dizhoor, A. M., and Ames, J. B. (2014) Structural diversity of neuronal calcium sensor proteins and insights for activation of retinal guanylyl cyclase by GCAP1. *Front. Mol. Neurosci.* **7,** 19
48. Lim, S., Strahl, T., Thorner, J., and Ames, J. B. (2011) Structure of a Ca^{2+}-myristoyl switch protein that controls activation of a phosphatidylinositol 4-kinase in fission yeast. *J. Biol. Chem.* **286,** 12565–12577
49. Hughes, R. E., Brzovic, P. S., Dizhoor, A. M., Klevit, R. E., and Hurley, J. B. (1998) Ca^{2+}-dependent conformational changes in bovine GCAP-2. *Protein Sci.* **7,** 2675–2680
50. Olshevskaya, E. V., Hughes, R. E., Hurley, J. B., and Dizhoor, A. M. (1997) Calcium binding, but not a calcium-myristoyl switch, controls the ability of guanylyl cyclase-activating protein GCAP-2 to regulate photoreceptor guanylyl cyclase. *J. Biol. Chem.* **272,** 14327–14333
51. Dell'Orco, D., Sulmann, S., Linse, S., and Koch, K. W. (2012) Dynamics of conformational Ca^{2+}-switches in signaling networks detected by a planar plasmonic device. *Anal. Chem.* **84,** 2982–2989
52. Stephen, R., Palczewski, K., and Sousa, M. C. (2006) The crystal structure of GCAP3 suggests molecular mechanism of GCAP-linked cone dystrophies. *J. Mol. Biol.* **359,** 266–275
53. Babu, Y. S., Bugg, C. E., and Cook, W. J. (1988) Structure of calmodulin refined at 2.2 Å resolution. *J. Mol. Biol.* **204,** 191–204
54. Zhang, M., Tanaka, T., and Ikura, M. (1995) Calcium-induced conformational transition revealed by the solution structures of apo calmodulin. *Nat. Struct. Biol.* **2,** 758–767
55. Gagné, S. M., Tsuda, S., Li, M. X., Smillie, L. B., and Sykes, B. D. (1995) Structures of the troponic C regulatory domains in the apo- and calcium-saturated states. *Nat. Struct. Biol.* **2,** 784–789
56. Peshenko, I. V., Olshevskaya, E. V., and Dizhoor, A. M. (2008) Binding of guanylyl cyclase activating protein 1 (GCAP1) to retinal guanylyl cyclase (RetGC1): the role of individual EF-hands. *J. Biol. Chem.* **283,** 21747–21757
57. Olshevskaya, E. V., Boikov, S., Ermilov, A., Krylov, D., Hurley, J. B., and Dizhoor, A. M. (1999) Mapping functional domains of the guanylate cyclase regulator protein, GCAP-2. *J. Biol. Chem.* **274,** 10823–10832
58. Ermilov, A. N., Olshevskaya, E. V., and Dizhoor, A. M. (2001) Instead of binding calcium, one of the EF-hand structures in guanylyl cyclase activating protein-2 is required for targeting photoreceptor guanylyl cyclase. *J. Biol. Chem.* **276,** 48143–48148
59. Olshevskaya, E. V., Ermilov, A. N., and Dizhoor, A. M. (1999) Dimerization of guanylyl cyclase-activating protein. *J. Biol. Chem.* **274,** 25583–25587
60. Ramamurthy, V., Tucker, C., Wilkie, S. E., Daggett, V., Hunt, D. M., and Hurley, J. B. (2001) Interactions within the coiled-coil domain of RetGC-1 guanylyl cyclase are optimized for regulation rather than for high affinity. *J. Biol. Chem.* **276,** 26218–26229
61. Yu, H., Olshevskaya, E., Duda, T., Seno, K., Hayashi, F., Sharma, R. K., Dizhoor, A. M., and Yamazaki, A. (1999) Activation of retinal guanylyl cyclase-1 by Ca^{2+}-binding proteins involves its dimerization. *J. Biol. Chem.* **274,** 15547–15555
62. Peshenko, I. V., Olshevskaya, E. V., Yao, S., Ezzeldin, H. H., Pittler, S. J., and Dizhoor, A. M. (2010) Activation of retinal guanylyl cyclase RetGC1 by GCAP1: stoichiometry of binding and effect of new LCA-related mutations. *Biochemistry* **49,** 709–717
63. Monod, J., Wyman, J., and Changeux, J. P. (1965) On the nature of allosteric transitions: a plausible model. *J. Mol. Biol.* **12,** 88–118